Effects of Ag and Sr dual ions implanted into SiC

T.T. Hlatshwayo[1*], N. Mtshonisi[1], E.G.Njoroge[1], M.Mlambo[1], M. Msimanga[2], V.A. Skuratov[3,4,5], J. H.O'Connell[6], J.B. Malherbe[1], S.V.Motloung[7,8]

[1]*Physics Department, University of Pretoria, Pretoria 0002, South Africa*

[2]*Physics Department, Tshwane University of Technology, P Bag X680, Pretoria 0001, South Africa*

[3]*Joint Institute for Nuclear Research, Dubna, Russia*

[4]*Dubna State University, Dubna, Moscow Region, Russia*

[5]*National Research Nuclear University MEPhI, Moscow*

[6]*Centre for HRTEM, Nelson Mandela University, Port Elizabeth, South Africa*

[7]*Department of Physics, Nelson Mandela University, P. O. Box 77000, Port Elizabeth 6031, South Africa*

[8]*Department of Physics, Sefako Makgatho Health Science University, P. O. Box 94, Medunsa, 0204, South Africa*

*corresponding author, TT Hlatshwayo. e-mail address: thulani.hlatshwayo@up.ac.za

Abstract

The effect of silver (Ag) and strontium (Sr) ions implanted into polycrystalline (SiC) was investigated. One batch of polycrystalline SiC wafers was implanted with 360 keV silver ions (Ag-SiC) and another implanted with 360 keV strontium ions (Sr-SiC). Both implantations were performed at 600 ^{o}C to a fluence of 2×10^{16} cm^{-2}. Some of the Ag- SiC samples were then implanted with Sr ions of 280 keV to a fluence of 2×10^{16} cm^{-2} at 600 ^{o}C (Ag&Sr-SiC). The as-implanted samples were annealed at temperatures from 1000 to 1400 ^{o}C in steps of 100 ^{o}C for 5 hours. The samples were thereafter characterised by Transmission electron microscopy (TEM), Raman spectroscopy, Elastic Recoil Detection Analysis (ERDA), Rutherford backscattering spectrometry (RBS), and Scanning electron microscopy (SEM). Both individual and dual implantations resulted in no amorphization of the SiC. As expected, dual implantation resulted in a higher defect concentration. Subsequent Sr implantation resulted in the formation of Ag precipitates, especially around grain boundaries. Annealing the Ag-SiC and Ag&Sr-SiC samples caused the shift of implants towards the surface accompanied by loss at 1400 ^{o}C while no loss was observed in the Sr-SiC samples.

Key words: SiC, Ag, Sr and implantation, Raman, radiation damage

Introduction

Excessive use of fossil fuels has contributed to a global rise in CO_2 levels and measurable climate change. Hence there is an urgent need for carbon neutral and environmental friendly methods of generating electricity. Wind, solar and nuclear energy are some proposed candidates [1]. Safety concerns and regulatory induced cost overhead has led to nuclear energy falling somewhat out of favour [2]. However, industrialisation which resulted in an increase in energy needs has recently revived consideration of nuclear energy around the world [3] [4].

In the pebble bed modular reactor (PBMR), the fuel consists of a fissile kernel coated by four chemical vapour deposited layers [5].The first layer is a porous carbon buffer. This layer accommodates internal gas build-up. The other three layers are the inner pyrolytic carbon (IPyC) layer that acts as a diffusion barrier to most non-metallic fission products (FPs), a silicon carbide (SiC) layer that acts as a main diffusion barrier to metallic FPs and an outer pyrolytic carbon (OPyC) layer that protects SiC. These coated particles retain most of the radiological important FPs with the exception of silver (^{110m}Ag), strontium (Sr) and europium (Eu) [6]. ^{110m}Ag is a strong gamma emitter with half-life of about 253 days [7] while owing to the chemical similarity of strontium with calcium, radioactive isotopes of strontium can cause radiological health concerns if released from reactors and be deposited in bones [8]. Extensive work has been done on the migration behaviour of Ag in SiC in temperatures ranging from nuclear reactor operation temperature (900 ^{o}C) to accidental temperature (1600 ^{o}C). These include out-of-pile release measurements from irradiated TRISO fuel [9-12], and ion implantation [13-17]. Little has been reported on the migration behaviour of Sr, and Eu in SiC [18-22]. In a nuclear reactor environment, fission products co-exist. Hence, to get more insight in the migration behaviour of these fission products in SiC, the migration behaviour of these important fission products needs to be investigated in the presence of others. However, less has been investigated regarding the synergetic effects of either Ag or Sr with other FPs. Only the synergistic effects of Ag and iodine (I) co-implanted in 6H-SiC [23]; palladium (Pd) and Ag in SiC [24] and ruthenium (Ru) and Ag have been investigated [25]. Iodine was found to play a role in the retainment of Ag while Pd and Ru assisted the migration of Ag. In this study the synergetic effect of Sr and Ag dual ions implanted into SiC is investigated. The results of this

study are crucial in understanding the migration behaviour of these fission products in an environment more closely resembling the nuclear reactor environment.

Experimental methods

Polycrystalline CVD-SiC wafers used in this study were obtained from Valley Design Corporation. The un-implanted SiC wafers were characterized by electron backscatter diffraction (EBSD) and x-ray diffraction (XRD). They were found to be composed of mainly 3C-SiC with some traces of 6H-SiC [13] [21]. Some of the samples were individually implanted with Ag ions of 360 keV to fluence of 2×10^{16} cm^{-2} at 600 ^{o}C (Ag-SiC) and Sr ions of 360 keV to a fluence of 2×10^{16} cm^{-2} at 600 ^{o}C (Sr-SiC) . The implantation temperature was above critical temperature to avoid amorphization. Some of the Ag implanted SiC were also implanted with Sr ions of 280 keV to a fluence of 2×10^{16} cm^{-2} at 600 ^{o}C (Ag&Sr-SiC). Ag-SiC, Sr-SiC, Ag&Sr-SiC samples were annealed at temperatures from 1000 to 1400 ^{o}C in steps of 100 ^{o}C for 5 hours. Ag-SiC, Sr-SiC and Ag&Sr-SiC samples were characterized by transmission electron microscopy (TEM), Raman spectroscopy, Elastic Recoil Detection Analysis (ERDA) and Rutherford backscattering spectrometry (RBS) while annealed samples were additionally characterized by scanning electron microscopy (SEM).

Cross-sectional TEM specimens were prepared using an FEI Helios Nanolab 650 FIB. Thinning of the samples were performed by successive 30 keV and 5 keV Ga ions. Finally, polishing was done at 2 keV and 500 eV which produced near damage free TEM foils. The TEM samples were analysed using a JEOL JEM 2100 LaB_6 transmission electron microscope operating at 200 kV.

Raman analysis was performed using a T64000 series II triple spectrometer system from HORIBA scientific from Jobin-Yvon using a 514.5 nm laser line as excitation source. Collection of the scattered light in backscattering geometry was made through an Olympus confocal microscope with a 50× objective lens attached. Finally the as-implanted and the annealed samples were analysed by ERDA at iThemba LABS TAMS. The ERDA technique detects recoil ions knocked off the surface region of a target sample by a projectile beam coming in at 20^{o} grazing incidence angle to the sample surface. The detector system employed was a Time of Flight – Energy (ToF-E) spectrometer. It consists of two carbon foil based timing detectors, 0.60 m apart, and a silicon PIPS® detector for measuring the energy of the recoil

ions in coincidence with their time of flight [26]. This coincidence measurement leads to separation of recoil particles according to their atomic mass. It is then possible to extract elemental energy spectra from the 2D ToF vs Energy plots and thence calculate depth profiles using an energy-depth conversion algorithm [27]. The profiles of the implanted species before and after annealing were obtained by Rutherford backscattering spectrometry (RBS) at room temperature using He^{1+} ions with energy of 1.6 MeV. The RBS experimental setup used in this study can be found in [13]. SEM was performed using a high-resolution Zeiss Ultra Plus 55 field emission scanning electron microscope (FESEM) operated at 2 kV.

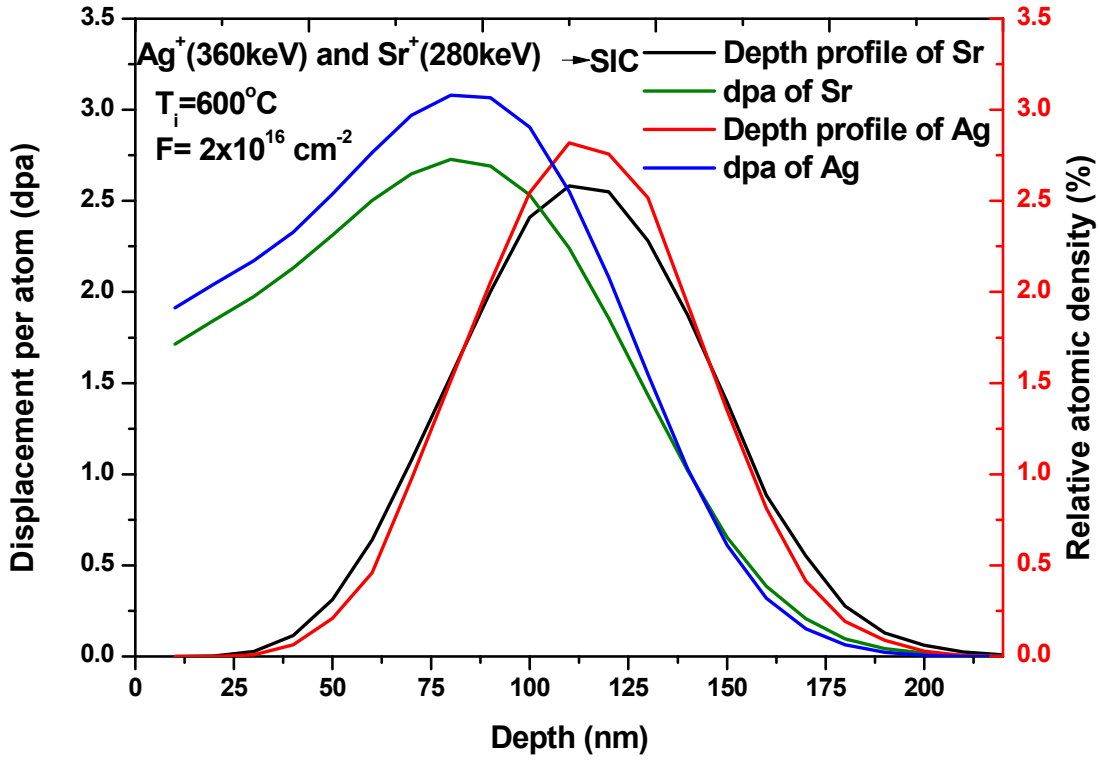

Fig.1: SRIM 2010 simulated depth profiles and displacement per atom (dpa) of Ag (360 keV) and Sr (280 keV) implanted into SiC.

Results and discussion

Fig.1 shows the depth profiles and displacement per atom (dpa) from SRIM 2010 calculation [28] of Ag (360 keV) and Sr (280 keV) implanted into SiC. The detailed calculation was used in both cases and the displacement energies of 35 and 20 eV for Si and C, respectively were adopted with density of 3.2 $g.cm^{-3}$[29]. What is evident from the results in Fig. 1 is that both

Ag and Sr have nearly the same projected range which allows the investigation of the synergetic effect of the two implanted species. Moreover, both ions produce maximum displacement damage between 75 – 100 nm depth.

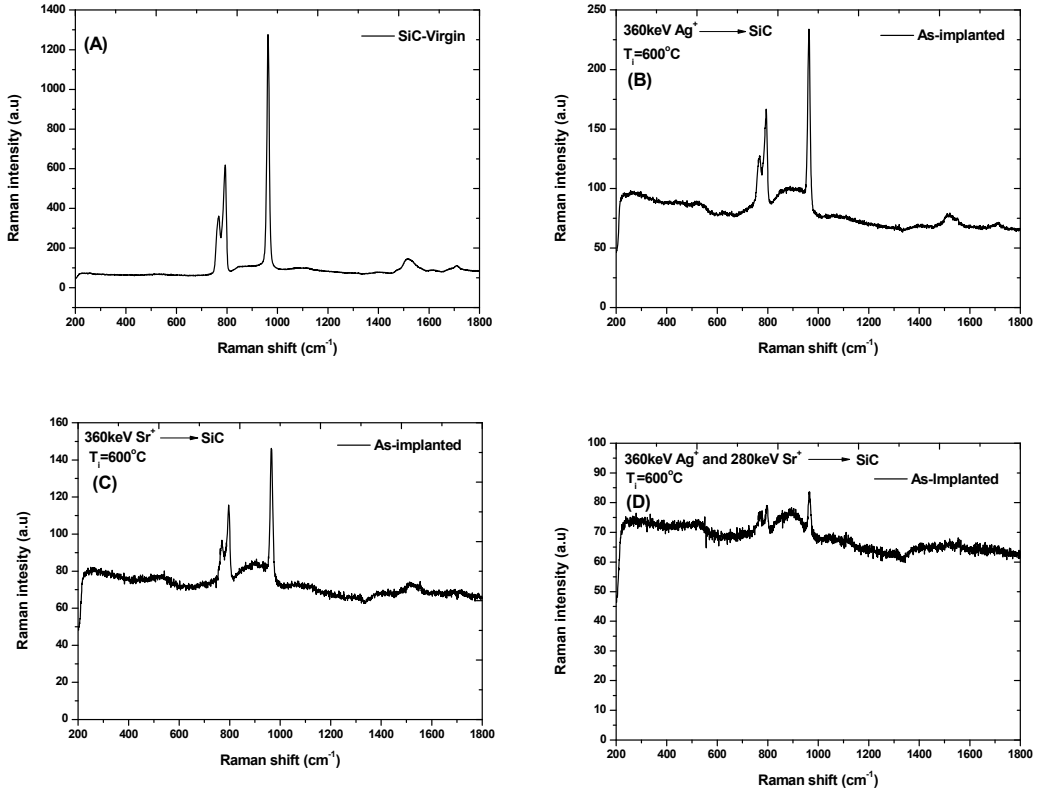

Fig.2: Raman spectra of Ag-SiC, Sr-SiC and Ag&Sr-SiC samples

The structural changes in Ag-SiC, Sr-SiC and Ag&Sr-SiC samples were investigated using Raman and TEM. Fig.2 shows the Raman spectra of Ag-SiC, Sr-SiC and Ag&Sr-SiC samples. The Raman spectrum of un-implanted/virgin sample is included for comparison. The virgin Raman spectrum in Fig 2 (a) has peaks at 794 and 968 cm^{-1} belonging to TO and LO phonon modes of cubic 3C-SiC and of 6H-SiC [30] [31]. These Raman results further confirm that the as received SiC samples were composed mainly of 3C-SiC with some traces of 6H-SiC as reported in [13] [21]. Both Ag and Sr individual and Ag and Sr dual implantations resulted in the reduction of SiC Raman characteristic peak intensities due to the defects retained after treatments, as shown in Fig 2 (b) and (c) respectively. The more pronounced reduction in the Raman spectrum of Ag&Sr-SiC samples (Fig 2(d)) indicates a higher defect concentration in

the dual implanted samples compared to single-ion implanted samples (Ag-SiC and Sr-SiC). The Ag&Sr-SiC samples were exposed to increased nuclear energy loss due to Ag ions and Sr ions which resulted in the interaction of defects. This interaction of defects resulted in more complex defects, hence more defective structure. Similar interaction of defects has been reported in SiC dual implanted with gold (Au) at 600 K and helium (He) at room temperature (RT) [32].The lack of amorphization in Ag-SiC, Sr-SiC and Ag&Sr-SiC samples is due to implantation temperature of 600 ^{o}C that is higher than amorphization critical temperature [33].

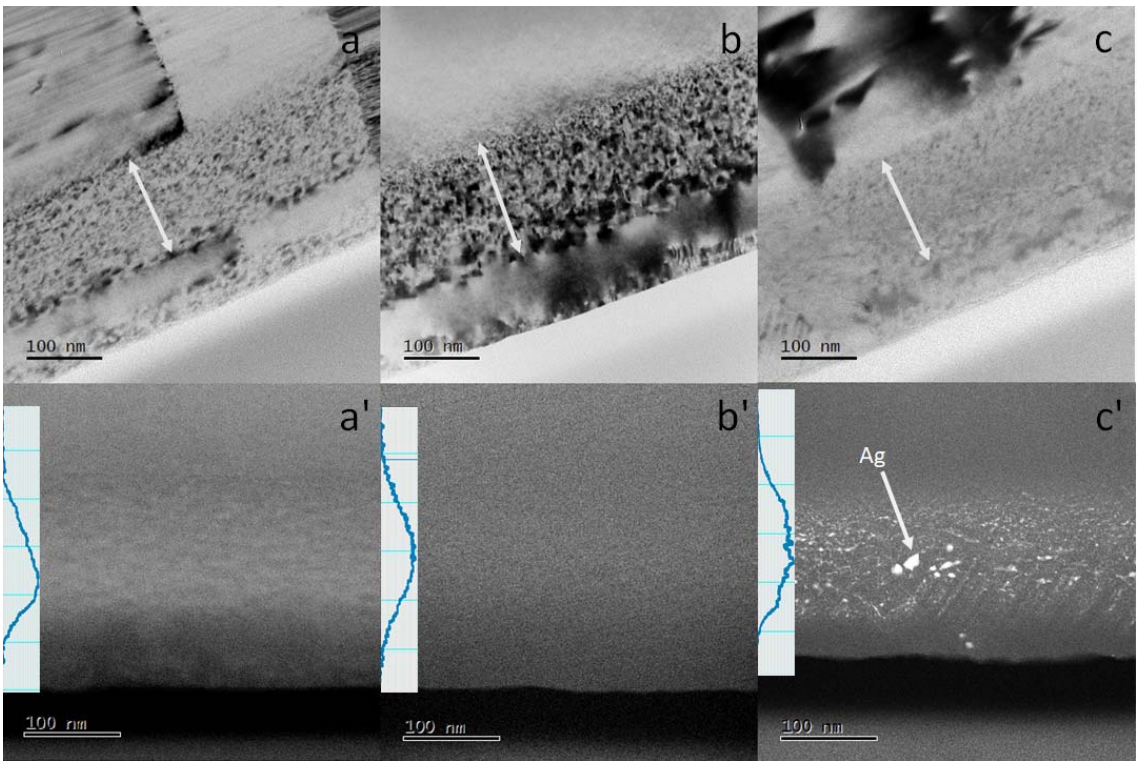

Fig.3: BF TEM and HAADFSTEM micrographs of Ag-SiC, Sr-SiC and Ag&Sr-SiC samples

Fig.3 shows bright field (BF) TEM and high-angle annular dark-field (HAADF) scanning TEM (STEM) micrographs of Ag-SiC, Sr-SiC and Ag&Sr-SiC samples. The bright field micrographs of Sr-SiC (a), Ag-SiC (b) and Ag&Sr-SiC (c) show highly defective implanted layers (indicated by the arrows in Fig.3). Dark contrasting strongly diffracting zones are present throughout the damaged region indicating that a high degree of crystallinity remained after implantation which is in agreement with the Raman results. HAADF micrographs of Sr-SiC (a') and Ag-SiC (b') show a slight increase in brightness through the projected range of the implanted ions but no metal precipitates could be observed. In contrast, the Ag&Sr-SiC

specimen (c') had a high density of metal precipitates several nm in size, especially concentrated around the edges of subgrains in the damaged region as well as along stacking faults. The inset plots on the HAADF images show normalized intensity profiles along the implantation direction. These plots have been corrected for the wedge shape of the lamellae through linear background subtraction. Energy dispersive x-ray spectroscopy (EDS) identified the inclusions as Ag. Therefore, implanted Ag rearranged and form precipitates in dual implanted samples. These precipitates might have been formed due to temperature effect during the implantation of Sr as Ag was the first ion implanted. Formation of Ag precipitates in Ag implanted SiC at RT after annealing first at 900 and 1250 °C has been reported in [14] and for other implanted species [33]. This precipitation only occurred after the as-implanted samples were vacuum annealed at very high temperature, cf. the 900 and 1250 °C quoted by [14]. The formation of Ag precipitates at a much lower temperature of 600 °C in the present study might be due to radiation-induced diffusion of the Ag atoms due to bombardment of Sr ions.

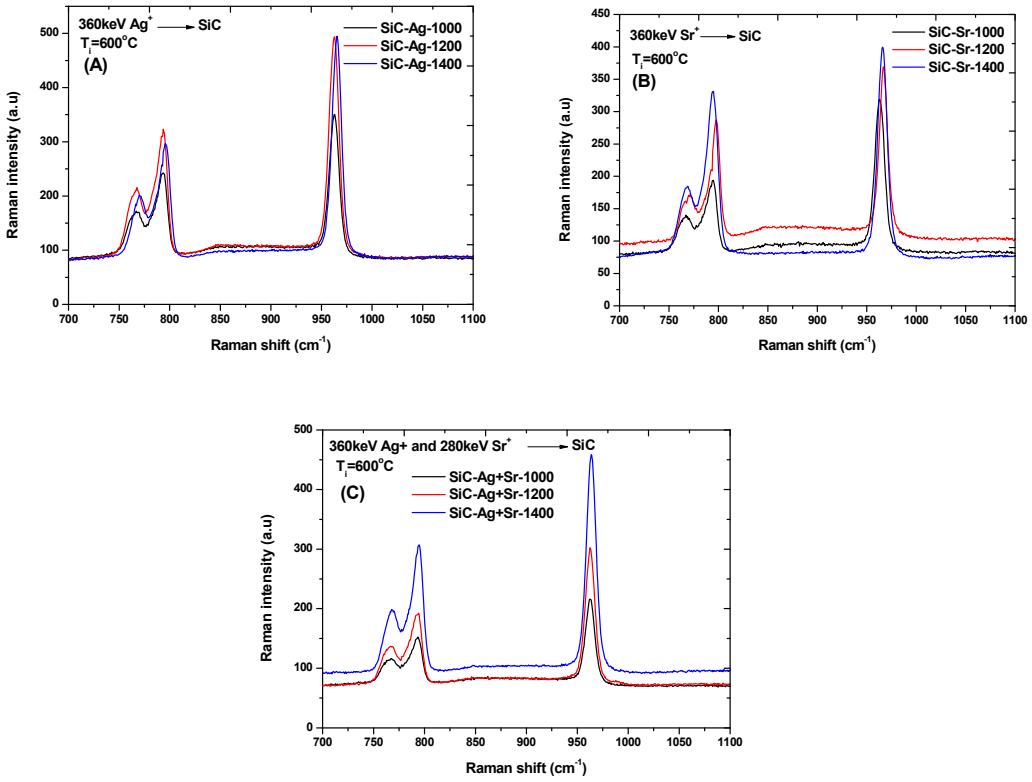

Fig.4: Raman spectra of Ag-SiC, Sr-SiC and Ag&Sr-SiC samples sequential annealed at temperatures from 1000 to 1400 °C in steps of 100 °C for 5 hours.

Raman spectroscopy was also used to investigate the annealing of defects in individual and dual implantations. Raman spectra of individual and dual implanted SiC then sequentially annealed at temperatures from 1000 to 1400 °C in steps of 100 °C for 5 hours are shown in Fig.4. Annealing at 1000 °C already caused an increase in intensities of SiC Raman characteristic peaks in all the samples indicating annealing of some defects. This annealing of defects progressed with increasing temperature up to 1400 °C. However, this increase in intensities seems to be more in Ag-SiC and Ag&Sr-SiC sample where Ag is present. These results might be indicating that Ag enhances annealing of defects in SiC as reported in [34] and increased crystalline growth [33].

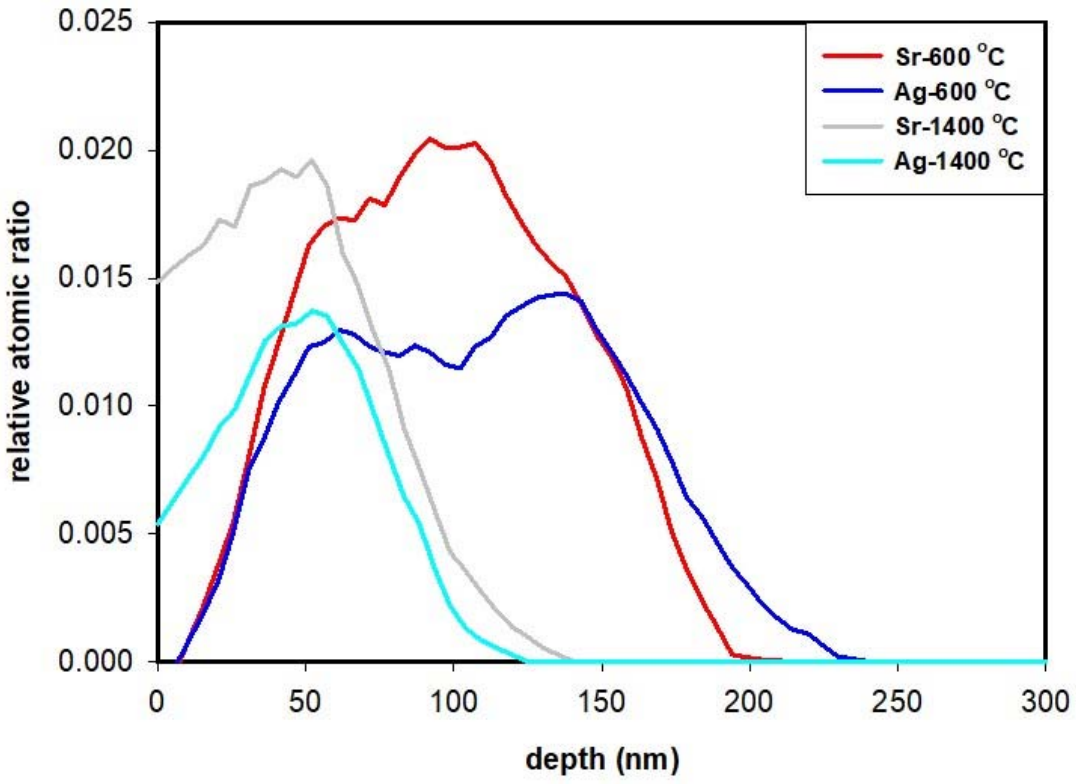

Fig.5: Ag and Sr depth profiles of the as-implanted and annealed Ag&Sr-SiC

The as-implanted Ag&Sr-SiC and Ag&Sr-SiC before and after sequentially annealed up to 1400 °C were characterized by ERDA. Fig. 5 shows the Ag and Sr depth profiles of the as-implanted and annealed Ag&Sr-SiC. The profile of the as implanted sample shows Ag and Sr profiles overlap with each other confirming the SRIM results in Fig.1. As expected, the as-

implanted Sr depth profile was almost Gaussian and symmetric, however the Ag profile consisted of double peak. This double peak profile might be an indication of silver forming precipitates in the dual implanted samples as was observed in TEM in Fig.3. Sequentially annealing up to 1400 °C caused both Ag and Sr to move towards the surface resulting in some loss of Ag and Sr.

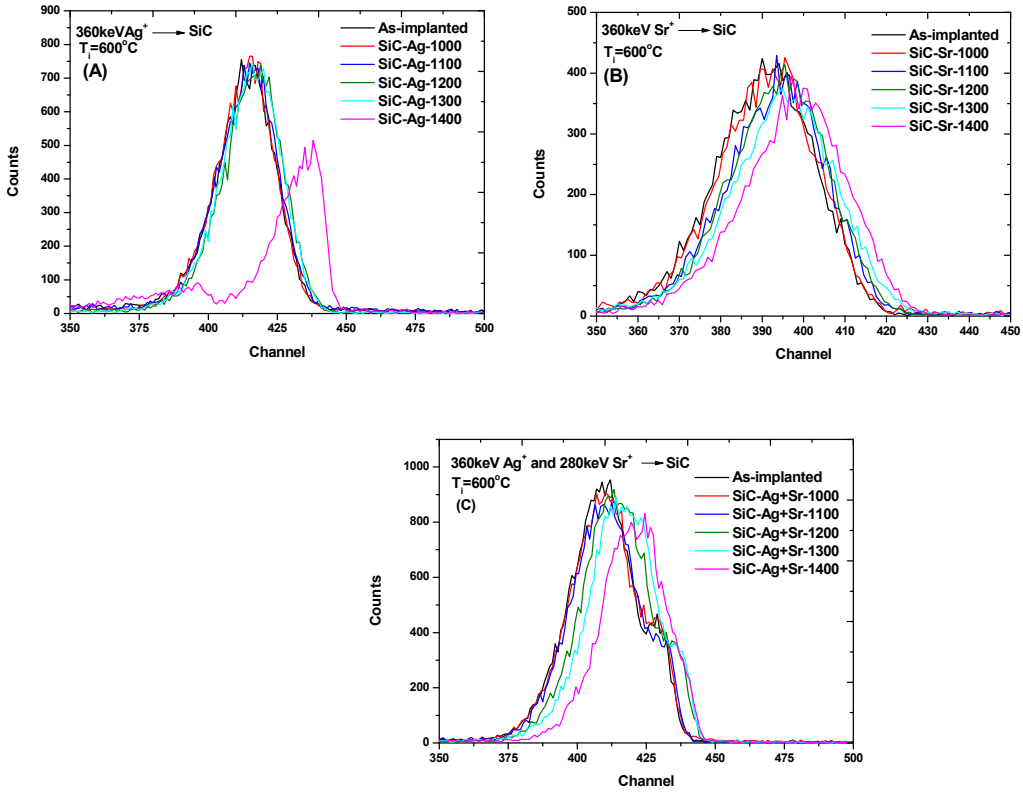

Fig.6: Rutherford backscattering spectrometry (RBS) profiles of implants after sequentially annealing from 1000 to 1400 °C in steps of 100 °C for 5 hours.

The migration behaviour in Ag-SiC, Sr-SiC and Ag&Sr-SiC samples were investigated after each annealing steps using RBS. The RBS profiles after sequentially annealing from 1000 to 1400 °C are shown in Fig.6 and their retained ratios are shown in Fig.7. Their as-implanted profiles are included in Fig.6 for comparisons. Both as-implanted RBS profiles of Ag-SiC and Sr-SiC are symmetric. The as-implanted RBS profile of Ag&Sr-SiC sample is asymmetric. This might be an effect of Ag forming precipitates which in agreement with TEM and ERDA results. Annealing at temperatures below 1200 °C caused no change in Ag-SiC and Ag&Sr-

SiC profiles, while in the Sr-SiC, Sr slightly shifted towards the surface accompanied by no loss. This shift of Sr towards the surface accompanied by no loss progressed with annealing temperature up to 1400 ^{o}C. Ag in the Ag-SiC samples and profile of the implants in Ag&Sr-SiC only shifted towards the surface after annealing at 1200 ^{o}C. These shifts were accompanied by loss of implants at 1400 ^{o}C in both samples. About 60% of implanted Ag was lost after annealing the Ag-SiC at 1400 ^{o}C while about 20% of the implants was lost in the Ag&Sr-SiC annealed at 1400 ^{o}C. Shifting of Sr towards the surface accompanied by no loss after sequential annealing Sr-SiC up to 1400 ^{o}C and the similar behaviour in the migration behaviour of the implants in Ag-SiC and Ag&Sr-SiC indicate the influence of Ag in the migration in the Ag&Sr-SiC samples.

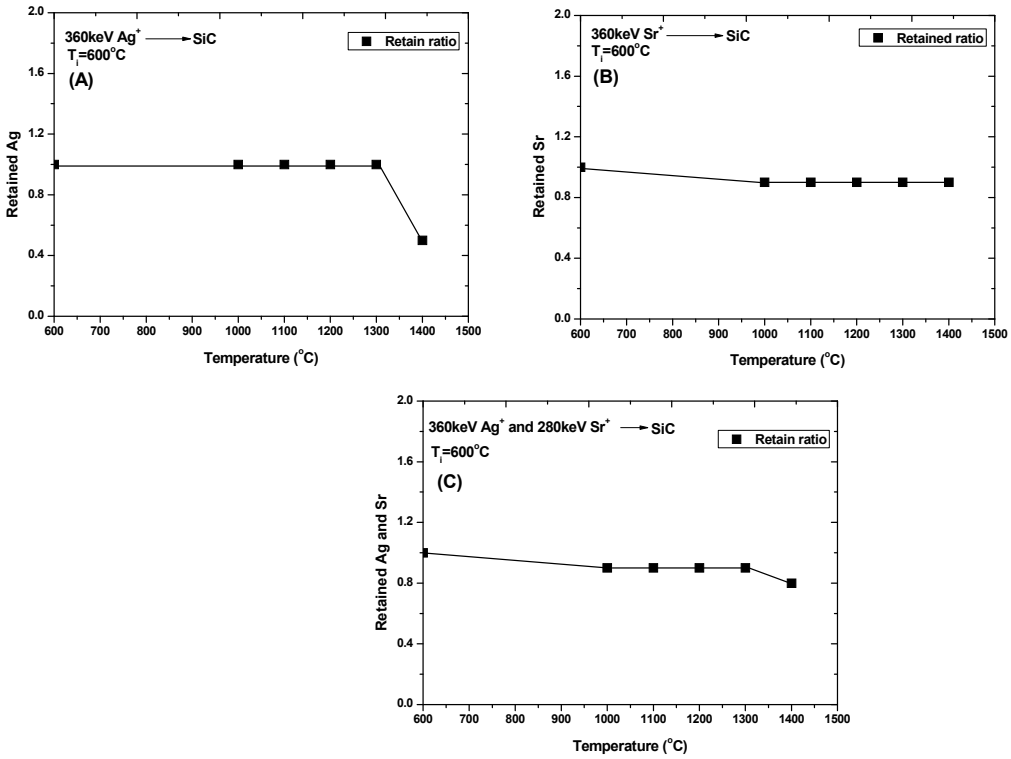

Fig7: The retained ratio of implants as a function of annealing temperature.

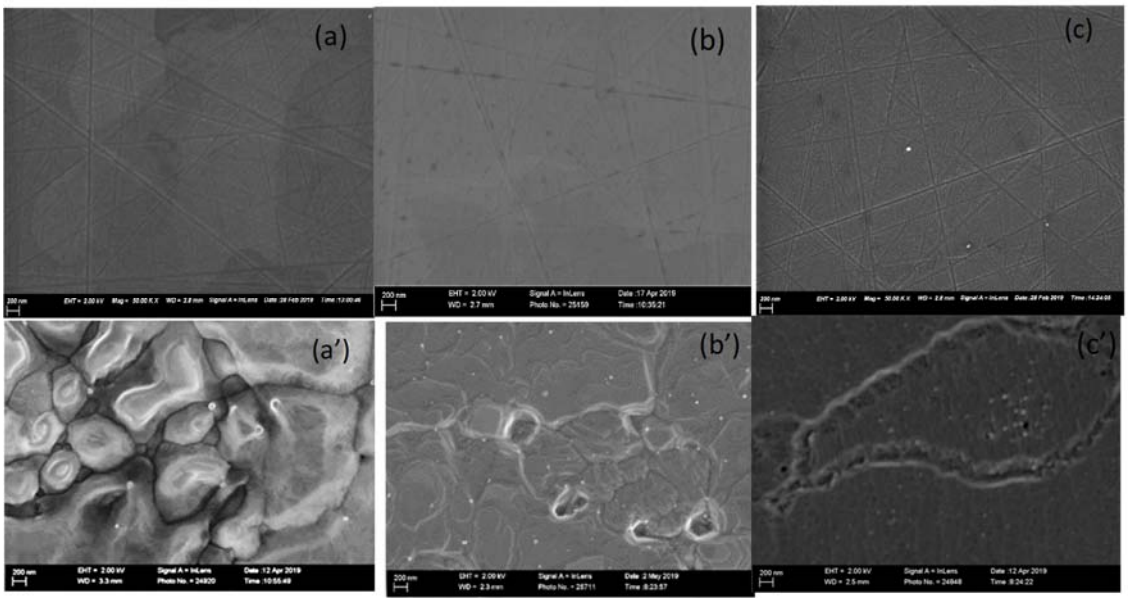

Fig.8: Scanning electron microscopy (SEM) micrographs of Ag-SiC, Sr-SiC and Ag&Sr-SiC and Ag-SiC, Sr-SiC and Ag&Sr-SiC sequential annealed up to 1400 ºC.

Scanning electron microscopy (SEM) micrographs of Ag-SiC, Sr-SiC and Ag&Sr-SiC and Ag-SiC, Sr-SiC and Ag&Sr-SiC sequential annealed up to 1400 ºC are shown Fig.8. SEM micrographs of Ag-SiC, Sr-SiC and Ag&Sr-SiC are relatively smooth with polishing marks on their surfaces. Usually room temperature as-implanted SiC samples exhibit a smooth surface due to swelling caused by amorphization leading to the disappearance of the polishing marks seen in as-receive samples [36]. These polishing marks seen in Fig. 8(a)-(c) indicate the lack of amorphization in all the implanted samples which is in agreement with the Raman and TEM findings. The annealed Ag-SiC sample in Fig 8(a') has much larger crystallites resulting in prostrutions with connected openings on the surface while annealed Sr-SiC has few holes that are not connected. Earlier it was alluded to the effect of Ag on improved SiC crystal growth [34]. The presence of implanted Sr atoms act as impurities inhibiting crystal growth in the dual implanted samples leading to smaller crystallites and smaller openings between the SiC crystallites in Fig. 8(b') and (c'). The interaction of implanted Ag with SiC at higher temperatures such as 1400 ºC is known to cause prostrutions and deeper holes that form silver escape paths [14]. Therefore, the loss of implanted species in Ag-SiC and Ag&Sr-SiC after annealing at 1400 ºC might be due to this interaction of silver with SiC resulting in openings which then allows the implants to escape.

Conclusions

The effect of Ag and Sr dual implanted into polycrystalline SiC has been investigated. For comparison purposes, Ag and Sr ions were individually implanted into SiC. Some of the Ag implanted SiC were then implanted with Sr ions. All implanted SiC were sequentially annealed at temperatures ranging from 1000 to 1400 ^{o}C in steps of 100 ^{o}C for 5 hours. Raman analysis revealed no amorphization in all implanted SiC with more defects retained in the dual implanted SiC. More defects were due to the interaction of defects retained by the Ag and Sr ions resulting in more complex defects. TEM results also confirmed the lack of amorphization and also revealed the formation of Ag precipitates in the dual implanted samples. The formation of Ag precipitates was due to Sr implantation. RBS and ERDA results also confirmed the formation of Ag precipitates in the dual implanted samples. Heat treatment caused annealing of defects with slightly pronounced annealing of defects in the Ag–SiC and Ag&Sr-SiC (as seen from the resulting high intensity Raman peaks) indicating that the presence of Ag enhances recrystallization. Annealing also resulted in the shifts of the implants toward the surface. These shifts were accompanied by loss of implanted species in Ag-SiC and Ag&Sr-SiC. This loss was found to be due to Ag interacting with SiC resulting in the formation of deeper holes that act as migration channels in the Ag-SiC and Ag&Sr-SiCsamples. These results point to the presence of Ag to have a role in the loss of implanted Sr. Therefore, in nuclear reactor where FPs co-exist, this role of Ag needs to be considered to achieve the total containment of Sr.

Declaration of Competing Interest

The authors declare that they have no known competing financial interests or personal relationships that could have appeared to influence the work reported in this paper.

Acknowledgement

The Authors would like to thanks Prof E Wendler and technical staffs at the Friedrich-Schiller-University Jena, Germany for implantations of the samples.

References

[1] Omer AM.. Journal of Soil Science and Environmental Management 2010;1:127–54.

[2] Hindmarsh R. Nuclear disaster at Fukushima Daiichi: social, political and environmental Issues. Routledge; 2013.

[3] Firoz Alam , Rashid Sarkar , Harun Chowdhury, Energy Procedia 160 (2019) 3–10

[4] Mark Ho, Edward Obbard, Patrick A Burr, Guan Yeoh, Energy Procedia 160 (2019) 459–466

[5] N. G. van der Berg, J. B. Malherbe, A. J. Botha and E. Friedland, Surf. Interface Anal. 42 (2010) 1156–1159.

[6] Internation atomic energy agency, (1997). Fuel performance and fission product behaviour in gas cooled reactors. [online] Available at: http://www .pub.iaea.org/books/IAEABooks/5633/Fuel-Performance-and-FissionProduct Behaviour-in-Gas-Cooled-Reactors [Accessed 8 Feb. 2017].

[7] P. Demkowicz, J. Hunn, R. Morris: Proceedings of the HTR 2012, Tokyo, Japan.

[8]D.Petti,J.Buongiorno,J.Maki,R.Hobbins,G.Miller,Key differences in the fabrication, irradiation and high temperature accidenttesting ofUSa nd German TRISO-coated particle fuel,and their implications on fuel performance,Nucl.Eng. Des.222(2–3)(2003)281–297.

[9] P.E. Brown, R.L. Faircloth, J. Nucl. Mater. 59 (1976) 29-41.

[10] H. Nabielek, P.E. Brown, P. Offermann, Nucl. Technol. 35 (1977)483-493.

[11] R.E. Bullock, J. Nucl. Mater. 125 (1984)304-319.

[12] J.J. van der Merwe, J. Nucl. Mater. 395 (2009)99-111.

[13] E. Friedland, J.B. Malherbe, N.G. van der Berg, T. Hlatshwayo, A.J. Botha, E. Wendler, W. Wesch, J. Nucl. Mater. 389 (2009) 326–331.

[14] T.T. Hlatshwayo , J.B. Malherbe , N.G. van der Berg , L.C. Prinsloo , A.J. Botha, E. Wendler , W. Wesch, Nucl. Instrum. Methods Phys. Res. B 274 (2012) 120–125.

[15] T.T. Hlatshwayo, J.B. Malherbe , N.G. van der Berg, A.J. Botha, P. Chakraborty, Nucl. Instrum. Methods Phys. Res. B 273 (2012) 61–64.

[16] H. J. MacLean, R. G. Ballinger, Second Topical Meeting on High Temperature Reactors 2004 (HTR-2004), Beijing, China, (2004) 22-24

[17]. H.A.A. Abdelbagi, V.A. Skuratov, S.V. Motloung, E.G. Njoroge, M. Mlambo, J.B. Malherbe, J.H. O'Connell, T.T. Hlatshwayo, Nucl. Instrum. Methods Phys. Res. B 461 (2019) 201–209

[18] E. Friedland,N.G. van der Berg, J.B. Malherbe, E. Wendler, W. Wesch, Journal of Nuclear Materials 425 (2012) 205–210.

[19] S. Dwaraknath, G. Was, J. Nucl. Mater. 444 (13) (2014) 170-174.

[20] H.A.A. Abdelbagi, V.A. Skuratov, S.V. Motloung, E.G. Njoroge, M. Mlambo, T.T. Hlatshwayo, J.B. Malherbe, Nuclear Inst. and Methods in Physics Research B 451 (2019) 113–121.

[21] S. Dwaraknath, G. Was, J. Nucl. Mater. 476 (2016) 155-167.

[22] T.M. Mohlala, T.T. Hlatshwayo, M. Mlambo, E.G. Njoroge, S.V. Motloung, J.B. Malherbe, Vacuum 141 (2017) 130-134

[23] T.T.Hlatshwayo,N.G.van der Berg, M.Msimanga, J.B.Malherbe, R.J.Kuhudzai, Nuclear Instruments and Methods in Physics Research B 334 (2014) 101–105

[24] H. Neethling, J.H. O'Connell, E.J. Olivier, Nucl. Eng. Design 251 (2012) 230.

[25] Jacques Herman O'Connell , Johannes Henoch Neethling Nucl. Mat. 456 (2015) 436-441.

[26] M. Msimanga, D. Wamwangi C.M. Comrie, C.A. Pineda-Vargas, M. Nkosi, T. Hlatshwayo , Nucl. Instrum. Methods Phys. Res. B 296 (2013) 54-60.

[27] A. Bergamier, G. Dollinger, C.M. Frey and T. Faestermann. J. Anal. Chem. 353

(1995) 582

[28] James F. Ziegler, M.D. Ziegler, J.P. Biersack, SRIM – The stopping and range of ionsin matter (2010), Nuclear Instrum. Meth. Phys. Res. B: Beam Interact. Mater. Atoms268 (11-12) (2010) 1818–1823,https://doi.org/10.1016/j.nimb.2010.02.091

[29] W.J. Weber, F. Gao, R. Devanathan, W. Jiang, The efficiency of damage production in silicon carbide, Nucl. Instrum. Meth. Phys. Res. B 218 (2004) 68.

[30] S. Nakashima, H. Harima, Phys. Stat. Sol. A 162 (1997)39,

[31] Z.C. Feng, W.J. Choyke and J.A. Powell, J. Appl. Phys. 64 (1988) 6827

[32] Xu Wang , Ziqiang Zhao, Ming Zhang, Yunbiao Zhao, Dong Han, Jian Chu, Yaping Sun, Honglong Wang and Sunli Liu, Mater. Res. Express 5 (2018) 105902

[33] Jiang W, Zhang Y and Weber W J 2004 Phys. Rev. B 70 (2004) 165208

[34] J.B. Malherbe, “Topical Review: Diffusion and radiation damage in 6H-SiC.” J. Phys. D Appl. Phys. 46 (2013) 473001

[35] Xin Geng, Fan Yang, Nadia Rohbeck, Ping Xiao, J. Am. Ceram. Soc., 97 (2014) 1979–1986

[36] J.B. Malherbe, N.G. van der Berg, A.J. Botha, E. Friedland, T.T. Hlatshwayo, R.J. Kuhudzai, E. Wendler, W. Wesch, P. Chakraborty and E.F. da Silveira, “SEM Analysis of Ion Implanted SiC”, Nucl. Instrum. Methods Phys. Res. B 315 (2013) 136 – 141